Transp Porous Med (2006) 65: 193–211
DOI 10.1007/s11242-005-6088-1

RESEARCH ARTICLE

Stability of a fluid in a horizontal saturated porous layer: effect of non-linear concentration profile, initial, and boundary conditions

H. Hassanzadeh · M. Pooladi-Darvish · D.W. Keith

Received: 20 September 2005 / Accepted: 25 November 2005

Abstract Carbon dioxide injected into saline aquifers dissolves in the resident brines increasing their density, which might lead to convective mixing. Understanding the factors that drive convection in aquifers is important for assessing geological CO_2 storage sites. A hydrodynamic stability analysis is performed for non-linear, transient concentration fields in a saturated, homogenous, porous medium under various boundary conditions. The onset of convection is predicted using linear stability analysis based on the amplification of the initial perturbations. The difficulty with such stability analysis is the choice of the initial conditions used to define the imposed perturbations. We use different noises to find the fastest growing noise as initial conditions for the stability analysis. The stability equations are solved using a Galerkin technique. The resulting coupled ordinary differential equations are integrated numerically using a fourth-order Runge–Kutta method. The upper and lower bounds of convection instabilities are obtained. We find that at high Rayleigh numbers, based on the fastest growing noise for all boundary conditions, both the instability time and the initial wavelength of the convective instabilities are independent of the porous layer thickness. The current analysis provides approximations that help in screening suitable candidates for homogenous geological CO_2 sequestration sites.

Keywords Stability analysis · Convection · Geological CO_2 storage · Saline aquifers · Geological sequestration

Nomenclature

A Time components of the perturbed velocity amplitude function
a Dimensionless wavenumber

H. Hassanzadeh · M. Pooladi-Darvish (✉)· D. W. Keith
Department of Chemical and Petroleum Engineering,
University of Calgary,
2500, University Drive, NW, Calgary, AB, Canada T2N 1N4
e-mail: pooladi@ucalgary.ca

B Time components of the perturbed concentration amplitude function
C Concentration [M/L^3]
$\bar{c}$ Amplification factor
$\boldsymbol{D}$ Molecular diffusion [L^2/T]
D Derivative operator
d Derivative
g Gravitational acceleration [L/T^2]
H Porous layer thickness [L]
I Integral function
i Imaginary number
k Permeability [L^2]
p Pressure [M/LT^2]
Ra Rayleigh number [Dimensionless]
t Time [T]
u Velocity in x-direction [L/T]
v Velocity in y-direction [L/T]
$\mathbf{v}$ Vector of Darcy velocity [L/T]
w Velocity in z-direction [L/T]
x Coordinate direction [L]
y Coordinate direction [L]
z Vertical coordinate direction [L]
α_D Decline factor [Dimensionless]
β Coefficient of density increase [L^3/M]
ϕ Porosity [Dimensionless]
λ Wavelength [L]
ρ Density [M/L^3]
μ Viscosity [M/LT]
$\Delta\rho$ Density difference [M/L^3]
∇_1^2 $\partial^2/\partial x_D^2 + \partial^2/\partial y_D^2$.

Subscripts
0 base state
c Critical
D Dimensionless
l Integral or summation index
m Integral or summation index
n Summation index

Superscripts
s Equilibrium state
‘ Perturbed state
* Amplitude of the perturbations

1 Introduction

The modeling of buoyancy-driven flow plays an important role in engineering disciplines such as atmospheric and ground water contaminant dispersion, reservoir engineering and geothermal reservoirs. The problem of hydrodynamic stability in porous media has been studied extensively (Horton and Rogers 1945; Lapwood 1948;

Morrison and Rogers 1949; Katto and Masuoka 1967; Beck 1972; Caltagirone 1980; Nield and Bejan 1999). The stability analysis for plain fluids under a variety of boundary conditions has also been thoroughly investigated (Morton 1957, Lick 1965, Foster 1965a,b, 1968, Mahler et al. 1968, Jhavery and Homsy 1982, Tan and Thorpe 1996). For example, Kaviany (1984) studied the onset of thermal convection in a porous medium both theoretically and experimentally. Kim et al. studied the onset of buoyancy-driven flow in porous media (Kim and Kim 2004, 2005). Ennis-King and Paterson (2003, 2005) performed a linear stability analysis to investigate the role of anisotropy on the onset of convection. Xu et al. (2006) performed convective stability analysis of the long term storage of CO_2 in deep saline aquifers to find the onset of convection. Riaz et al. (2006) also used linear stability analysis based on the dominant mode of the self-similar diffusion operator and numerical simulations to find a scaling relationship for the onset of convection.

Different methods have been used for characterizing time-dependent concentration or temperature profiles including linear amplification theory, the energy method, and the non-linear amplitude method (Kaviany 1984). Onset time predicted by the energy method is almost one order of magnitude less than actual measured laboratory data (Wankat and Homsy 1977), while the linear amplification theory gives values that are more closely agree with the experimental values (Foster 1965a, b; Kaviany 1984). The CO_2 injected into a saline aquifer is less dense than the resident brine. Driven by density contrasts, CO_2 will flow up and then horizontally (in a horizontal aquifer), spreading under the cap rock, and will potentially leaking through any high permeability zones or artificial penetrations such as abandoned wells. The free-phase CO_2 (gas or supercritical fluid) slowly dissolves and diffuses into the formation brine. The diffusion of CO_2 into underlying formation brine increases the density of brine near the top of the aquifer, bringing the system to a hydro-dynamically unstable state. Instabilities can arise from the combination of an unstable density profile and inherent perturbations within the system. Such instabilities, if created, cause convective mixing and greatly accelerate the dissolution of CO_2 into the aquifer (Lindeberg and Wessel-Berg 1996, Ennis-King and Paterson 2003, Ennis-King et al. 2005, Hassanzadeh et al. 2005). This process has timescale of order of a century. While the gas remains in free-phase, there is a risk of leakage arising from strong buoyancy-driven flow. Assessments of the risk of leakage of CO_2 from a storage formation may need to consider leakage mechanisms and their likelihood of occurrence during the full time period over which mobile, free-phase CO_2 is expected to remain in the reservoir. Convective mixing increases the rate of dissolution and therefore decreases the time scale over which leakage is possible. Once CO_2 is dissolved, risk assessments may well ignore the leakage pathways resulting from the very slow movement of CO_2-saturated brines, caused by background aquifer flow. Therefore, developing suitable criteria for the onset of convection is important in the design and implementation of large scale geological CO_2 storage in saline aquifers (IPCC Report, 2005).

In this work, the lower and upper bounds of the onset of instability in porous media are investigated based on initial condition dependency of the amplitude functions. In particular, the analysis is performed for the time-dependent concentration field with time-dependent and time-invariant boundary conditions. Although stability analysis has been studied widely, it is of interest to investigate the role of initial and boundary conditions on the onset of buoyancy-driven convection in porous media when a time-dependent concentration field exists. Three boundary conditions which are most relevant to CO_2 storage are studied. In all cases, the domain is initially free of

CO_2 and is fully saturated with brine. The first case is constant CO_2 concentration at the top and zero-flux condition at the bottom boundary. In the second case, the top boundary condition is similar to the one applied in the first case, but the bottom boundary is zero-concentration rather than zero-flux. The third case is a linear ramp decrease in CO_2 concentration with a decline factor α_D at the top boundary, while the bottom boundary is maintained at zero CO_2 concentration. In all three cases the domain is homogenous, laterally infinite, and closed to flow from top and bottom. The first boundary condition is more relevant to the geological CO_2 sequestration in saline aquifers where a cap of CO_2 is brought into contact with the formation brine. In this case the concentration of CO_2 in the CO_2-brine interface is constant. The second boundary condition, which is the classical boundary condition of thermal convection (Horton and Rogers 1945; Lapwood 1948), has theoretical importance and therefore merits investigation. The third boundary condition examines the effect of ramp decrease in top boundary concentration on the onset of convection. This boundary condition represents a case where the pressure of the injected CO_2 in the gas cap decreases with time in a linear fashion. The pressure decline in the gas cap causes a decline in the equilibrium concentration at the CO_2-brine interface in a time-dependent manner. In all three cases, the contact between the CO_2-free phase and formation brine is taken as a boundary condition to simplify and cast the problem as one of a single-phase flow. It has been shown that in the presence of basic flow, transverse dispersion retards the onset of convection, when the stability analysis is performed based on linear temperature or concentration profile (Rubin 1974, Weber 1975, Tyvand 1977, Kvernvold and Tyvand 1980). The effect of transverse dispersion that might affect the onset of convection is neglected in this study. In another study, we have shown that in the presence of basic flow, transverse dispersion will also slow down the onset of convection for non-linear concentration profile (Hassanzadeh 2006).

The results presented here provide approximations that help in screening CO_2 storage sites. From a theoretical point of view, the present analysis can be applied to any problem in which the instabilities evolve in a transient concentration or temperature field. The paper is organized as follows. First, a stability analysis is presented for each of the three different cases. Next, the solution methodology to obtain the onset of convection is described and the results of the analysis are presented and discussed. Data from acid gas injection sites in the Alberta basin, as an analogue for geological CO_2 sequestration, are then examined to investigate the incidence of natural convection. Finally, we provide a summary of the major results.

2 Stability analysis

The physical model and the coordinate system used in this study are shown in Fig. 1. The model is a homogenous, porous medium with thickness H, saturated with brine, closed to flow from below the bottom of the aquifer. The lateral extent is infinite and the fluid is initially quiescent. The domain is exposed to a change in solute (CO_2) concentration from the top at time zero. Due to diffusion of CO_2, the formation brine becomes denser than the resident brine. As is well known, such a top-heavy arrangement is unstable to certain perturbations when the Rayleigh number exceeds a critical value. The Boussinesq approximation and Darcy model are assumed to be valid. For such a system, the governing equations of flow and the concentration field expressed by employing the Darcy model for the fluid velocity are given by

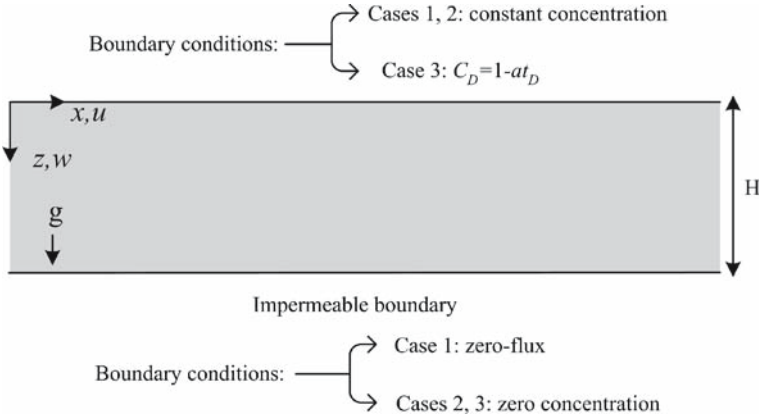

Fig. 1 A schematic diagram of the three cases considered

$$\nabla \cdot \mathbf{v} = 0, \tag{1}$$

$$\mathbf{v} = -\frac{k}{\mu}(\nabla p - \rho g \nabla z), \tag{2}$$

$$\boldsymbol{D}\phi\nabla^2 C - \mathbf{v} \cdot \nabla C = \phi\frac{\partial C}{\partial t}, \tag{3}$$

$$\rho = \rho_r(1 + \beta C), \tag{4}$$

where $\mathbf{v}$ is the vector of Darcy velocity; t is time; k is permeability; ϕ is porosity; p is pressure; C is the local, time-dependent CO_2 concentration; ρ_r is the resident brine density; ρ is the local, time-dependent CO_2-saturated brine density; μ is viscosity; β is the coefficient of density increase with respect to CO_2; $\boldsymbol{D}$ is the CO_2 molecular diffusion coefficient, and z is the vertical coordinate, which is positive downwards.

The stability of such a system is given by the Rayleigh number for a porous medium:

$$Ra = \frac{kg\Delta\rho H}{\mu\phi\boldsymbol{D}}, \tag{5}$$

where H is the porous layer thickness, $\Delta\rho = \beta C^s \rho_r$ is the density difference between CO_2-saturated brine at initial condition and the fresh aquifer brine, and C^s is the initial equilibrium concentration of CO_2 at the brine-CO_2 interface. The mass transfer is initially diffusive without any free convective motion. We define this flow as the *base state* which is governed by the following partial differential equation as given by

$$\frac{\partial^2 C_{0D}}{\partial z_D^2} = \frac{\partial C_{0D}}{\partial t_D}, \tag{6}$$

$$C_{0D} = C_0/C^s, z_D = z/H, \quad t_D = \boldsymbol{D}t/H^2, \tag{7}$$

where C_0 is the base concentration, C_{0D} is the dimensionless base concentration, and t_D is the dimensionless time.

We now analyze the stability of the base case in three different situations, given by three sets of boundary conditions. The first situation considers constant concentration on top of the aquifer and zero-flux at the bottom boundary. In the second situation, the top boundary condition is similar to the one applied in the first situation, but the bottom boundary is kept at a zero-concentration condition. The third situation represents the stability analysis for a ramp (linear) decrease in CO_2 concentration at the top boundary while the bottom boundary is maintained at zero CO_2 concentration. Transient stability analysis presented in this study follows previous works (Foster 1965a, 1968, Mahler et al. 1968, Ennis-King and Paterson 2003, Ennis-King et al. 2005, Kim and Kim 2005).

Case 1: Step change at the top and closed at the bottom: The initial and boundary conditions for this case are:

$$C_{0D} = 0 \quad \text{at} \quad t_D = 0, \quad 0 \le z_D \le 1, \tag{8}$$

$$C_{0D} = 1 \quad \text{at } z_D = 0, \quad t_D \ge 0, \tag{9}$$

$$\frac{\partial C_{0D}}{\partial z_D} = 0 \quad \text{at } z_D = 1, \quad t_D \ge 0. \tag{10}$$

Solution can be obtained by separation of variables as given by Ozisik (1993):

$$C_{0D} = 1 - \frac{4}{\pi} \sum_{n=1}^{\infty} \frac{1}{(2n-1)} \sin\left(\frac{(2n-1)}{2} \pi z_D\right) \exp\left(-\left(\frac{2n-1}{2}\right)^2 \pi^2 t_D\right).$$

The base velocity components are given by

$$u_0 = v_0 = w_0 = 0, \tag{11}$$

where u_0, v_0 and w_0 are longitudinal, lateral, and vertical base velocity components, respectively.

Perturbation equations: The concentration and velocity are subjected to infinitesimal perturbations. The perturbed fields C', v', u', w' are defined as $C = C_0 + C'$ etc. Neglecting the products of the infinitesimal terms, the governing equations of flow and concentration (Eqs. 1 and 3) may be written in terms of perturbed quantities as follows:

$$\nabla^2 w' = \frac{gk\Delta\rho}{\mu} \nabla_1^2 C' \quad , \tag{12}$$

$$\boldsymbol{D}\phi \nabla^2 C' - w' \frac{\partial C_0}{\partial z} = \phi \frac{\partial C'}{\partial t}. \tag{13}$$

Let us use the following dimensionless quantities as given by

$$x_D = x/H, \quad y_D = y/H, \quad w'_D = w'H/\phi \boldsymbol{D}, \quad \text{and} \quad Ra = kg\Delta\rho H/\mu \boldsymbol{D}\phi.$$

Introducing the above dimensionless parameters results in the following equations:

$$-\nabla^2 w'_D = Ra \nabla_1^2 C', \tag{14}$$

$$\nabla^2 C' - w'_D \frac{\partial C_0}{\partial z_D} = \frac{\partial C'}{\partial t_D}. \tag{15}$$

Boundary conditions: The boundary conditions for the perturbed flow and concentration are given by

$$w'_D = w_D = 0 \quad \text{at } z_D = 0, \quad z_D = 1, \quad \text{and} \quad t_D \geq 0, \tag{16}$$

$$\frac{\mathrm{d}^2 w'_D}{\mathrm{d}z^2} = \frac{\mathrm{d}^2 w_D}{\mathrm{d}z^2} = 0 \quad \text{at} \quad z_D = 0, \qquad z_D = 1, \quad \text{and} \quad t_D \geq 0, \tag{17}$$

$$C'_D = 0 \quad \text{at } z_D = 0, \quad \text{and} \quad t_D \geq 0, \tag{18}$$

$$\frac{\partial C_D{}'}{\partial z_D} = 0 \quad \text{at } z_D = 1, \quad \text{and} \quad t_D \geq 0. \tag{19}$$

Amplitude equations: The perturbed velocity and concentration may be expressed as:

$$\begin{bmatrix} w'_D\,(t_D, x_D, y_D, z_D) \\ C'_D\,(t_D, x_D, y_D, z_D) \end{bmatrix} = \begin{bmatrix} w^*_D\,(t_D, z_D) \\ C^*_D\,(t_D, z_D) \end{bmatrix} \exp\left[i\left(a_x x_D + a_y y_D\right)\right], \tag{20}$$

where the parameters with superscripted asterisks represent the amplitude of the perturbed quantities, $a = \left(a_x^2 + a_y^2\right)^{1/2}$ is the horizontal dimensionless wave number, and i is the imaginary number.

Introducing perturbed quantities into Eqs. 14 and 15 produces the following system of differential equations for the amplitude functions of velocity and concentration:

$$\left(\mathrm{D}^2 - a^2\right) w^*_D = -a^2 Ra C^*_D, \tag{21}$$

$$\left(\mathrm{D}^2 - a^2\right) C^*_D - w^*_D \frac{\partial C_0}{\partial z_D} = \frac{\partial C^*_D}{\partial t_D}, \tag{22}$$

where $\mathrm{D} = \mathrm{d}/\mathrm{d}z_D$.

By making use of the Galerkin technique, the amplitude functions are represented by a system of linearly independent functions satisfying the boundary conditions (Foster 1965b, Mahler et al. 1968, Ennis-King and Paterson 2003, Ennis-King et al. 2005, Kim and Kim 2005).

$$w^*_D = \sum_{l=1}^{N} A_l\,(t_D) \sin\left(l\pi z_D\right), \tag{23}$$

$$C^*_D = \sum_{l=1}^{N} B_l\,(t_D) \sin\left(\frac{(l-1)}{2}\pi z_D\right). \tag{24}$$

Introducing the above equations into the amplitude equations and using the orthogonality property gives:

$$E_{ml} A_l\,(t_D) = F_{lm} Ra B_l\,(t_D), \tag{25}$$

$$W_{lm} \frac{\mathrm{d}B_l}{\mathrm{d}t_D} = R_{lm} B_l - 2J_{ml} A_m, \tag{26}$$

where

$$E_{lm} = \delta_{lm}((l\pi)^2 + a^2), \tag{27}$$

$$F_{lm} = \frac{8a^2 m\,(-1)^{m-l+1}}{\pi\,(-1+2l-2m)\,(-1+2l+2m)}, \tag{28}$$

$$W_{ml} = \delta_{lm}, \tag{29}$$

$$R_{lm} = -\delta_{lm}\left(\left(\frac{(2l-1)\,\pi}{2}\right)^2 + a^2\right), \tag{30}$$

$$J_{ml} = \int_0^1 \frac{\partial C_{0D}}{\partial z_D} \sin\left(l\pi z_D\right) \sin\left(\frac{(2m-1)\,\pi z_D}{2}\right) \mathrm{d}z_D, \tag{31}$$

where δ_{lm} is the Kronecker delta and E, F, W, J, and R are $\mathbf{N} \times \mathbf{N}$ matrices.

It can be shown that:

$$J_{lm} = \frac{1}{2}\left[\exp\left(-\left(\frac{(2\,(m-l)-1)}{2}\right)^2 \pi^2 t_D\right) - \exp\left(-\left(\frac{2\,(l+m)-1}{2}\right)^2 \pi^2 t_D\right)\right]. \tag{32}$$

Using Eqs. 25 and 26 and elimination of $A_l\,(t_D)$ results in

$$\frac{\mathrm{d}B_l\,(t_D)}{\mathrm{d}t_D} = G_{lm} B_l\,(t_D)\,, \tag{33}$$

where $\boldsymbol{G}$ is an $\mathbf{N} \times \mathbf{N}$ matrix expressed by

$$G_{lm} = \mathbf{W}^{-1}[\mathbf{R} - Ra\mathbf{J}\mathbf{E}^{-1}\mathbf{F}]. \tag{34}$$

The system of $\mathbf{N}$ ordinary differential equations given by Eq. 33 should be solved numerically using standard methods to evaluate the growth of the initial perturbations.

Case 2: Step change at the top and zero-concentration at the bottom: For this case, the initial and boundary conditions are:

$$C_{0D} = 0 \quad \text{at } t_D = 0, \quad \text{and} \quad 0 \le z_D \le 1, \tag{35}$$

$$C_{0D} = 1 \quad \text{at } z_D = 0, \quad \text{and} \quad t_D \ge 0, \tag{36}$$

$$C_{0D} = 0 \quad \text{at } z_D = 1, \quad \text{and} \quad t_D \ge 0. \tag{37}$$

The solution can be obtained by separation of variables as given by Ozisik (1993):

$$C_{0D} = 1 - z_D - 2\sum_{n=1}^{N} \frac{1}{n\pi} \sin\left(n\pi z_D\right) \exp\left(-n^2\pi^2 t_D\right). \tag{38}$$

The basic state for velocity components and the derivation of amplitude functions are similar to the previous case. In deviation from the previous case the bottom boundary condition is given by

$$C'_D = 0, \quad \text{at } z_D = 1, \quad \text{and} \quad t_D \ge 0. \tag{39}$$

Similar to the previous case, by making use of the Galerkin technique, the amplitude functions are represented by a system of linearly independent functions satisfying the boundary conditions (Foster 1965b, Mahler et al. 1968, Kim and Kim 2005).

$$w_D^* = \sum_{l=1}^{N} A_l\,(t_D)\sin\,(l\pi\, z_D), \tag{40}$$

$$C_D^* = \sum_{l=1}^{N} B_l\,(t_D)\sin\,(l\pi\, z_D). \tag{41}$$

Introducing the above equations into the amplitude Eqs. 14 and 15 and using orthogonality gives the following two equations:

$$\left((l\pi)^2 + a^2\right) A_l\,(t_D) = a^2 Ra B_l\,(t_D), \tag{42}$$

$$\frac{\mathrm{d}B_l}{\mathrm{d}t_D} = -\left((l\pi)^2 + a^2\right) B_l - 2\sum_{m=1}^{N} A_m I_{lm}, \tag{43}$$

where in deviation from the previous case:
for $m = l$:

$$I_{lm} = -\frac{1}{2}\left(1 - \exp\left(-4l^2\pi^2 t_D\right)\right) \tag{44}$$

for $m \neq l$:

$$I_{lm} = \frac{1}{2}\left[\exp\left(-\,(l+m)^2\,\pi^2 t_D\right) - \exp\left(-\,(l-m)^2\,\pi^2 t_D\right)\right]. \tag{45}$$

As time approaches infinity, I_{lm} for $m \neq l$ goes to zero and I_{ml} for $m = l$ becomes

$$I_{ll} = -\frac{1}{2}. \tag{46}$$

It can be shown that, in this case, solving Eqs. 42 and 43 for the long-time gives:

$$Ra = \frac{\left((l\pi)^2 + a^2\right)^2}{a^2}. \tag{47}$$

Horton and Rogers (1945) found that for a linear steady-state temperature distribution, there exists a critical Rayleigh number $Ra_c = 4\pi^2$, above which perturbations grow and convection occurs, and below which the perturbations decay. Steady-state solution for the boundary condition of Case 2 is a linear concentration distribution. Equation 47, which is the special case for Eqs. 42 and 43 when time goes to infinity, leads to the critical Rayleigh number $Ra_c = 4\pi^2$, corresponding to a dimensionless wave number of $a = \pi$ for $l = 1$ as obtained by Horton and Rogers (1945).

Similar to the previous cases, Eqs. 42 and 43 generate a system of ordinary differential equations that are needed to estimate the growth of the initial perturbations.
Case 3: Ramp contact: The initial and boundary conditions for this case are given by

$$C_{0D} = 1 - \alpha_D t_D \quad \text{at } z_D = 0 \quad \text{where } 0 \le t_D \le 1/\alpha_D, \tag{48}$$

$$C_{0D} = 0, \quad \text{at } z_D = 1, \quad \text{and} \quad t_D \ge 0 \tag{49}$$

with initial condition of

$$C_{0D} = 0, \quad t_D \geq 0, \quad \text{and} \quad 0 \leq z_D \leq 1. \tag{50}$$

The solution to the base case can be obtained by Duhamel's theorem as given by Carslaw and Jaeger (1959)

$$C_{0D} = (1 - \alpha_D t_D)(1 - z_D) + \sum_{n=1}^{N} \frac{2\alpha_D}{(n\pi)^3} \sin(n\pi z_D) \left[1 - \exp\left(-n^2\pi^2 t_D\right)\right] - \sum_{n=1}^{N} \frac{2}{(n\pi)} \sin(n\pi z_D) \exp\left(-n^2\pi^2 t_D\right). \tag{51}$$

The basic state for velocity components and the derivation of amplitude functions and their boundary conditions are similar to the previous case.

Using similar functions as in the previous case for the velocity and concentration amplitudes, we obtain:

$$\frac{\mathrm{d}B_l}{\mathrm{d}t_D} = -((l\pi)^2 + a^2)B_l - 2\sum_{m=1}^{N} A_m I_{lm}, \tag{52}$$

$$((l\pi)^2 + a^2)A_l(t_D) = a^2 Ra B_l(t_D), \tag{53}$$

where

$$I_{lm} = \int_0^1 \frac{\partial C_{0D}}{\partial z_D} \sin(m\pi z_D) \sin(l\pi z_D)\, \mathrm{d}z_D. \tag{54}$$

Incorporating Eq. 51 into Eq. 54, it can be shown that in deviation from the previous cases:
for $m = l$:

$$I_{lm} = \frac{1}{2}\exp\left(-4l^2\pi^2 t_D\right) - \frac{1}{2}(1 - \alpha_D t_D) - \frac{\alpha_D}{2\pi^2}\frac{\left[1 - \exp\left(-4l^2\pi^2 t_D\right)\right]}{4l^2} \tag{55}$$

for $m \neq l$:

$$I_{lm} = \frac{\alpha_D}{2\pi^2}\left\{\frac{\left[1 - \exp\left(-(l-m)^2\pi^2 t_D\right)\right]}{(l-m)^2} - \frac{\left[1 - \exp\left(-(l+m)^2\pi^2 t_D\right)\right]}{(l+m)^2}\right\} + \frac{1}{2}\left[\exp\left(-(l+m)^2\pi^2 t_D\right) - \exp\left(-(l-m)^2\pi^2 t_D\right)\right]. \tag{56}$$

Similar to the previous cases Eqs. 52 and 53 make a system of ordinary differential equations that can be solved to evaluate the growth of the initial perturbations.

3 Solution methodology

In all three cases presented above, the system of **N** ordinary differential equations are integrated using a fourth-order Runge-Kutta method (Gerald and Wheatley 1989).

Determination of the coefficients $A_l(t_D)$ and $B_l\,(t_D)$, along with Eqs. 23 and 24 or 40 and 41, gives the amplitude of the disturbances. Such disturbances may either grow (or decay) with time.

As suggested by Foster (1965a, 1968), one can define an amplification factor of the averaged disturbances based on the amplitude of the velocity perturbation:

$$\overline{c} = \left\{ \int_0^1 w_D^{*2}\,(z_D, t_D)\,\mathrm{d}z_D \Big/ \int_0^1 w_D^{*2}\,(z_D, 0)\,\mathrm{d}z_D \right\}^{1/2}. \tag{57}$$

Our stability analysis examines the time evolution of this amplification factor $\overline{c}$. The results of the stability analysis depend on two factors. The first is the initial condition for the amplitude noise, and the second is the criterion set for determining the onset of convection from the study of variations of the amplification factor with time. We shall choose the most stringent conditions for the onset of convection and then present the band of conditions that may correspond to the onset of instability. We first describe the role of these factors in determining the onset of convection.

In order to solve the system of ordinary differential equations, initial conditions are needed for the perturbation amplitude. Foster (1965a, 1968), studied the growth of disturbances and found that a white noise spectrum of amplitude perturbations gives a faster rate of growth for a case in which a fluid cools from above. For a fluid-saturated porous medium heated from below, Kim and Kim (2005) found that a noise with only the lowest wave number in the amplitude spectrum gives the fastest growth rate. Foster (1965a, b) proposed that the onset of convection will be manifested when the average velocity disturbance has increased by a factor between one and three orders of magnitude. He has also shown that the choice of growth factor which defines the critical time has little effect on the determination of the critical wave number. In the following section, we present results of the stability analysis using different spectra of the amplitude function to find the lower and upper bounds of the onset of convection. Four different noises that cover a wide range of wave numbers in the amplitude spectrum are used as initial conditions: white noise in which all wave numbers of the amplitude spectrum are present, a noise with only the lowest wave number present, a noise with only the fourth component present, and a noise with only the tenth component present.

The effects of choice of amplitude function as initial conditions on the critical times for the three aforementioned cases are presented. Convergence analysis shows that 10–20 terms in the amplitude spectrum are sufficient at low Rayleigh numbers. However, at high Rayleigh numbers, large numbers of terms in the amplitude spectrum are needed for convergence. Two criteria have been chosen for determining the onset of instability. The first criterion is the critical time when the amplification factor is at a minimum, designated as the intrinsic instability time, and is represented by $\partial\overline{c}/\partial t_D = 0$. The second criterion is when the disturbances grow and reach an amplification factor of one, designated as the marginal instability time, and is represented by $\overline{c} = 1$ (Kim and Kim 2005). We define the intrinsic instability time as the lower bound and the marginal instability time as the upper bound on the timescale for the onset of instability in this study. It is noted that the marginal instability defined here is only an approximation for the upper bound.

To find the critical time and the corresponding critical wave number for a specified Rayleigh number the following procedure is used. Using a fixed Rayleigh number

and a specified noise type, marginal and intrinsic instability times are evaluated for different wave numbers. Minimizing the resulting times versus wave number gives the critical time and the associated critical wave number. The smallest critical time which is obtained by minimization of intrinsic instability time corresponds to the lower bound timescale for the onset of instability. On the other hand, the largest critical time which is obtained by minimization of the marginal instability time versus wave number corresponds to the approximate upper bound timescale. Therefore, for a fixed Rayleigh number and a specified noise, critical wave number, the lower bound, and the upper bound of instability are obtained. Using the aforementioned procedure, only one point in the critical time-Rayleigh number or the critical wave number-Rayleigh number space is obtained. In order to construct the t_{Dc}-Ra or a_c-Ra curve that covers a wide range of Rayleigh numbers, one needs to perform a similar calculation for all Rayleigh numbers of interest. In the following section, we use the above method to construct the critical parameter relationships.

4 Results and discussion

Figure 2(a) shows results for dimensionless critical time (for onset of convection) versus Rayleigh number for Case 1, in which a porous layer is subjected to a constant concentration boundary condition from the top and is closed from the bottom. The critical time in this figure corresponds to the critical wave number that results in the smallest critical time. Figure 2(a) shows that both dimensionless intrinsic instability and dimensionless marginal instability times are inversely proportional to Ra^2 at high Rayleigh numbers. Since the dimensionless critical time is inversely proportional to the porous layer thickness H to the power of 2, this means that the onset of convection is independent of porous layer thickness. In Fig. 2, the filled and open circles show intrinsic and marginal stability times, respectively. Figure 2(b) shows the effect of different noises as initial conditions on the instability time. In this case, the white noise grows faster than other noises. Results reveal that for each noise, the upper bound is typically two to three times the lower bound.

Figure 2(c) shows the dimensionless critical time versus Rayleigh number for Case 2 in which the porous layer is exposed to a constant concentration from the top and zero concentration from the bottom. The analogous problem has been solved by Caltagirone (1980) for thermal convection in a porous layer. Results in Fig. 2(c) reveal that both dimensionless intrinsic instability and dimensionless marginal instability times vary as the minus 2 power of the Rayleigh number at high Ra. Since the dimensionless critical time is inversely proportional to the porous layer thickness H, to the power of 2, this suggests that, the onset of convection is independent of porous layer thickness. Similar observations were reported by Caltagirone (1980). In Fig. 2(d), there is also data from Caltagirone (1980) for comparison, shown by open and closed diamonds for intrinsic and marginal stability times, respectively. Figure 2(d) shows the effect of different noises on the instability time. Similar to the previous case, the white noise promotes the fastest growing instabilities as compared to other noises studied. Also similar to the previous case, results show that for each noise, the upper bound is typically two to three times the lower bound. Another remark regarding Fig. 2(c) is that the minimum Rayleigh number approaches $4\pi^2$, corresponding to the critical Rayleigh number given by Horton and Rogers (1945) for a porous layer with a steady linear temperature gradient.

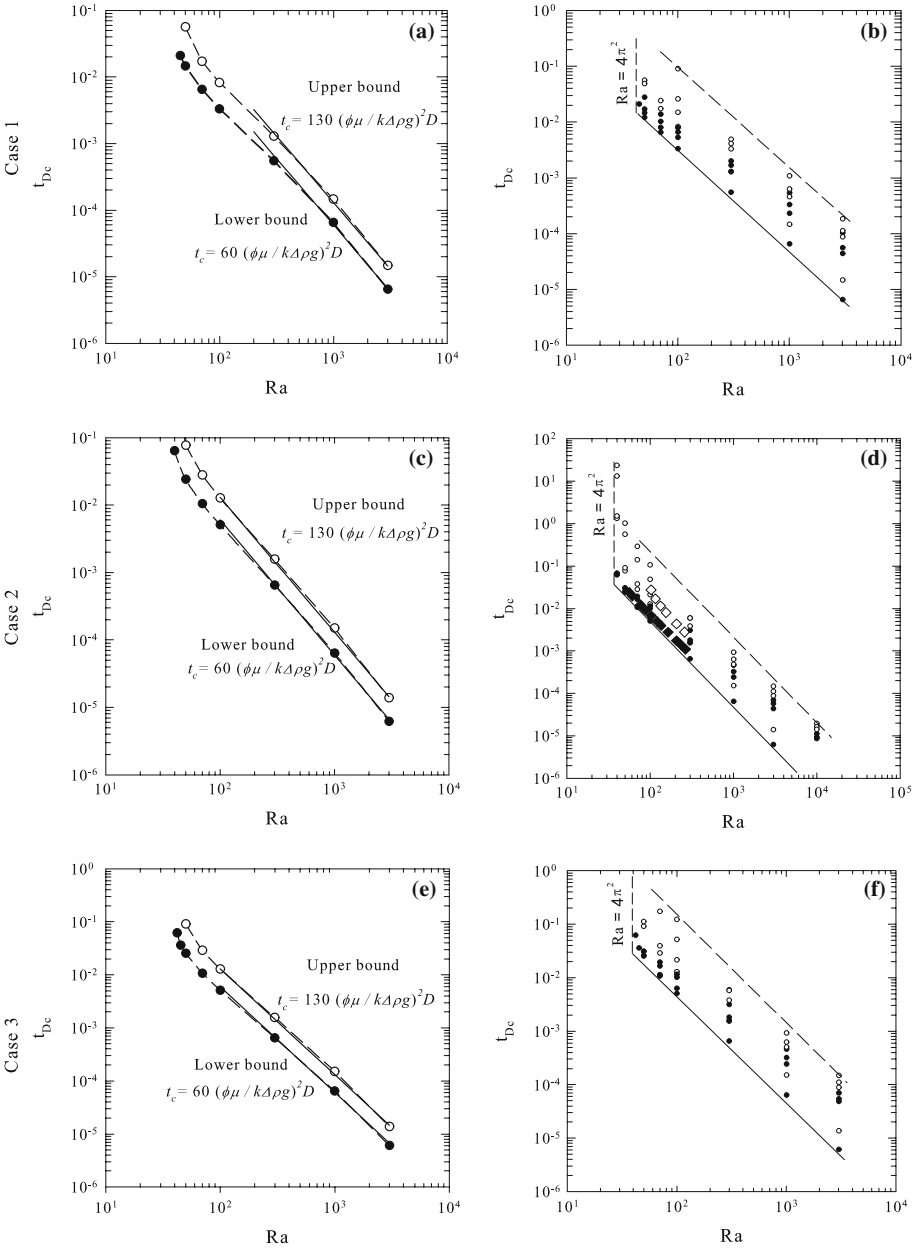

Fig. 2 Dimensionless intrinsic and marginal instability times versus Rayleigh number based on fastest growing perturbation as initial condition for all boundary conditions (left). In all cases white noise is the fastest growth noise. Intrinsic and marginal instability time versus Rayleigh number for all noises (right). Filled and open circles show intrinsic and marginal instability time, respectively. In (d) filled and open diamonds are data reported by Caltagirone (1980) shown for comparison for intrinsic and marginal stability times, respectively

Figure 2(e) shows the dimensionless critical time versus Rayleigh number for Case 3, where the porous layer is exposed to a linear ramp decrease in CO_2 concentration at the top boundary while the bottom boundary is maintained at zero CO_2 concentration. In the presented results, the decline factor of unity is assumed. Similar to the previous cases, the white amplitude noise promotes the fastest growing instability as compared to other noise spectra studied. Results clearly show that both dimensionless intrinsic instability and dimensionless marginal instability times vary inversely as the *Ra* squared at high Rayleigh numbers, suggesting that the onset time of convection is independent of porous layer thickness. Results for all initial conditions (noises) are given in Fig. 2(f). Similar to the previous cases, results here also demonstrate that for each noise the upper bound is typically two to three times the lower bound. Figure 2 shows that all boundary conditions result in similar t_{Dc}-*Ra* scaling behavior at high Rayleigh numbers.

Figure 3 shows the effect of decline factor on growth of perturbations as a function of dimensionless time for three Rayleigh numbers. The wave numbers used in calculations corresponded to the critical wave number at low decline factor for the Rayleigh numbers. Results demonstrate how increasing the decline factor could potentially weaken the perturbation and thereby eliminate convection. Figure 3 demonstrates that for $Ra = 500$, increasing the decline factor does not affect the intrinsic and marginal instability time. Results for the two other Rayleigh numbers illustrate that increasing the decline factor affects the growth of the perturbation significantly. Therefore, using a large decline factor at low Rayleigh numbers prevents a perturbation from growing and eliminates the conventional instabilities.

As mentioned in the previous section, at each critical time, there is a corresponding critical wave number at which the onset time is at a minimum. This wave number determines the size of the convection cells. Results in Fig. 4 show the critical dimensionless wave number versus Rayleigh number for white amplitude noise as the initial condition. The critical dimensionless wave number is defined as $2\pi H/\lambda$ where λ is wavelength. This figure reveals that, in all cases, the wave number is proportional to the Rayleigh number for *Ra* larger than a few hundred. This proportionality implies that the size of convection cells is independent of the porous layer thickness. As expected, the Rayleigh number of $4\pi^2$ leads to a minimum dimensionless wave number of π.

In the following section, the analysis developed herein is used to determine the onset of convection in the Alberta basin aquifers and the corresponding wavelengths of the convective instabilities.

5 Applications

Analysis of the conditions that drive convective instability may provide useful input in choosing suitable candidate sites for CO_2 storage. In choosing suitable candidates for large scale geological CO_2 sequestration, the onset of convection is quite important. Natural convection leads to improved dissolution of CO_2 in formation brine, making it less buoyant than the in situ brine. Therefore, an aquifer with a lower onset time of convection implies likely lower risk of CO_2 leakage through the natural and artificial pathways and is therefore more favorable.

Data from 24 acid gas injection sites in the Alberta basin, representing analogues for CO_2 sequestration, are used to estimate the lower bound for the onset of convection and the corresponding wavelengths of the dominant convective instabilities.

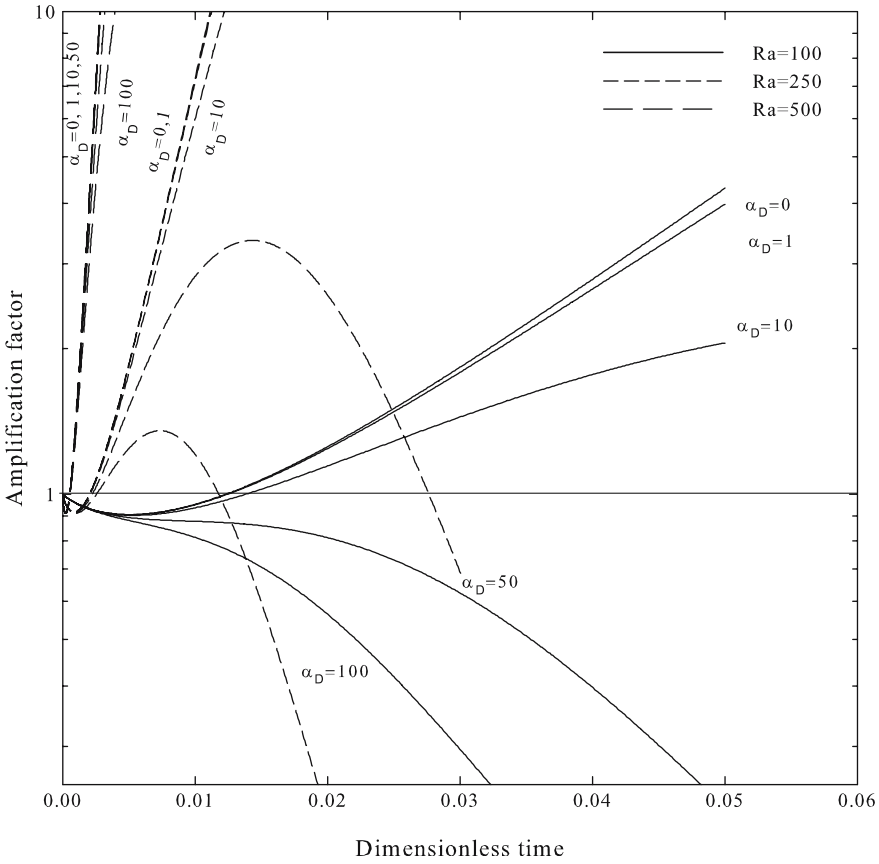

Fig. 3 Effect of decline factor α_D on growth of perturbations as a function of dimensionless time for three Rayleigh numbers: 100, 250, 500

The acid gases being injected in 24 storage sites in the Alberta basin are a mixture of CO_2 and H_2S. We used this data as an analogue for pure CO_2 storage cases since dissolution of H_2S in formation brine does not increase the brine density and therefore does not contribute to convective mixing. The Rayleigh numbers are calculated using data provided by Bachu et al. (2005) and Bachu Carroll (2005) for these 24 injection sites in the Alberta basin. A thermodynamic module is used to calculate the thermodynamic and transport properties (Hassanzadeh 2006). In all cases, the formation was assumed homogenous. While formation heterogeneity could have a large effect on formation of convective instabilities, in the absence of theoretical criteria for instability in heterogeneous formations, we used those developed in this paper. Table 1 gives the calculated Rayleigh numbers, onset of convection, and the corresponding wavelengths for the acid gas injection sites in Alberta basin aquifers.

Table 1 shows that the calculated *Ra* numbers are greater than $4\pi^2$ in 14 of the 24 sites investigated. Therefore, more than 50% of the injection sites would likely undergo convection in the long term, leading to improved dissolution of CO_2. Ten sites indicate pure diffusive mixing, corresponding to cases with low Rayleigh numbers. The lower bound of onset of convection varies from a fraction of a year to a

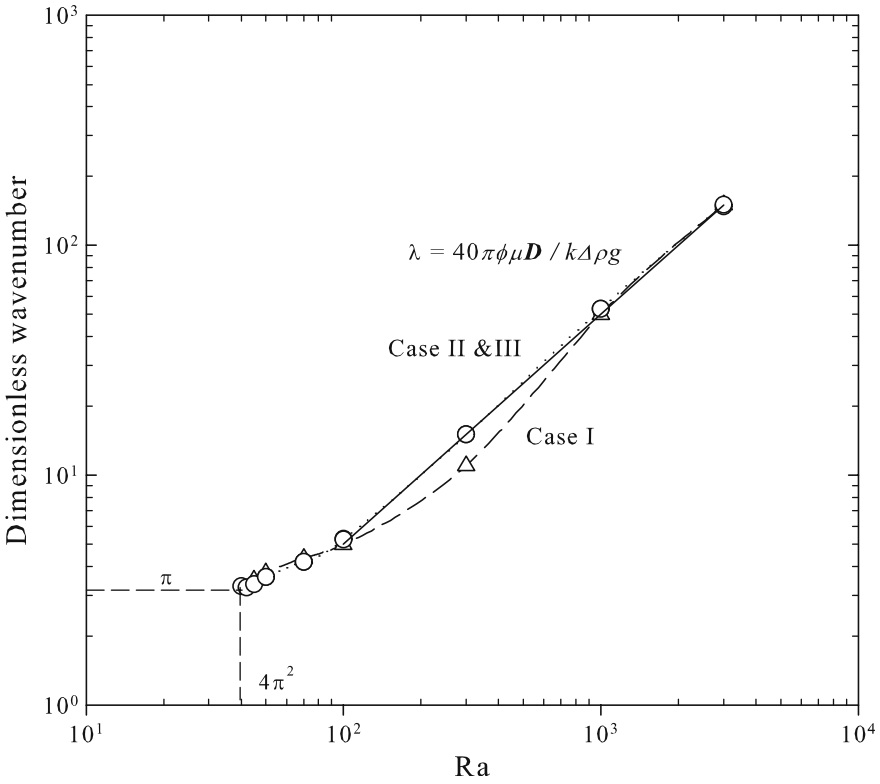

Fig. 4 Critical dimensionless wave number as a function of Rayleigh number for three cases studied, based on white amplitude noise as the initial condition

maximum of 40 years. The minimum and maximum wavelengths of the instabilities are 2 and 45 m, respectively.

In case 3 we have investigated the effect of a gradual decrease in equilibrium concentration of CO_2 on the onset of convection. Results show that a high decline factor can potentially eliminate the convection at low Rayleigh numbers and therefore need to be accounted in choosing a suitable candidate site for geological CO_2 storage.

The stability analysis presented can be used for validating numerical models used for large scale, density-driven flow simulations in geological formations. Large scale, density-driven flow simulations based on geological models require large numbers of grid blocks to achieve appropriate resolution and are therefore quite computationally expensive to run. Accurate modeling of density-driven flow, such as the convective mixing encountered in geological storage of CO_2, requires appropriate grid block size selection to capture the instabilities which evolve during the process. Results presented herein—i.e., the wavelengths of instabilities—can be used to define appropriate numerical discretization in flow simulations. Furthermore, in some storage sites, the wavelengths of the instabilities are very small, posing a numerical challenge in accurately modeling large scale flow simulations in such geological formations.

Table 1 Calculated Rayleigh number, the lower bound of the onset of convection, and the corresponding approximate initial wavelengths of the convective instabilities for 24 acid gas injection sites in the Alberta basin

Site	k (mD)	ϕ	μ (mPa s)	$\boldsymbol{D}$ (m^2/s)	$\Delta\rho^{b}$ (kg/m^3)	H (m)	Ra	t_c-*lower* (yr)	λ (m)
1	30	0.06	0.60	4.1×10^{-9}	4.65	15	142	5.17	14
2	186	0.18	0.66	4.0×10^{-9}	3.56	10	139	2.46	10
3	40	0.05	0.78	3.9×10^{-9}	1.58	18	74	28.38	28
4	100	0.10	0.65	3.7×10^{-9}	4.30	8	141	1.63	7
5	16	0.07	0.64	5.1×10^{-9}	1.51	10	11	pd[a]	
6	30	0.12	0.50	5.5×10^{-9}	3.22	13	38	40.07	
7	6	0.13	0.74	3.2×10^{-9}	4.41	4	3	pd	
8	9	0.04	0.67	3.7×10^{-9}	4.28	81	318	33.65	33
9	6	0.20	0.63	4.2×10^{-9}	3.42	29	11	pd	
10	9	0.12	0.46	4.5×10^{-9}	8.90	9	29	pd	
11	137	0.09	0.36	7.6×10^{-9}	4.09	60	1359	1.05	9
12	75	0.06	0.39	7.4×10^{-9}	3.40	10	146	1.21	6
13	115	0.08	0.48	5.0×10^{-9}	6.10	10	364	0.29	4
14	9	0.12	0.44	5.5×10^{-9}	6.15	10	19	pd	
15	14	0.06	1.32	2.7×10^{-9}	0.00	10	0	pd	
16	67	0.22	0.82	2.6×10^{-9}	6.03	40	351	9.68	15
17	346	0.10	0.60	3.7×10^{-9}	5.33	4	329	0.08	2
18	10	0.11	0.61	4.5×10^{-9}	3.37	24	27	pd	
19	13	0.12	0.65	4.3×10^{-9}	2.82	13	14	pd	
20	32	0.12	0.57	4.3×10^{-9}	4.78	13	67	16.45	20
21	27	0.05	0.63	5.0×10^{-9}	1.85	40	127	37.56	45
22	109	0.06	0.55	4.6×10^{-9}	4.53	5	162	0.39	4
23	1	0.12	0.48	5.9×10^{-9}	3.46	26	3	pd	
24	130	0.10	0.52	5.5×10^{-9}	2.94	10	133	1.93	10

[a] Pure diffusion

[b] Density difference between CO_2 saturated brine and fresh brine

6 Conclusions

A linear stability analysis has been performed for three transient concentration fields in a homogenous, saturated, porous medium. Using the amplification factor theory, the critical time-Rayleigh number and the critical wave number-Rayleigh number relationships are obtained. The approximate upper and lower bounds for the onset of convection obtained in this analysis could help in choosing suitable candidates for CO_2 storage sites. In addition, the initial wavelength of the convective instabilities can be used for appropriate grid block selection in flow simulations. The following conclusions can be drawn from this study.

- Results demonstrate that for each noise the marginal stability time is two to three times the intrinsic instability time.
- For all boundary conditions studied, at high Rayleigh numbers the onset of convection and the initial wavelength of the convective instabilities are independent of porous layer thickness.
- In all cases, white noise is the dominant noise character of perturbations that causes convection.

- The steady decrease in top boundary concentration with a high decline factor has a stabilizing effect.
- Results from 24 acid gas injection sites in the Alberta basin aquifers, as an analogue for CO_2 storage, reveal that greater than 50% of those sites will experience convection over the long term.

Acknowledgements The financial support for this work was provided by the National Science and Engineering Research Council of Canada (NSERC) and by the Alberta Department of Energy. Computer facilities were provided through a CFI grant. This support is gratefully acknowledged. The first author also thanks the National Iranian Oil Company (NIOC) for financial support.

References

Bachu, S., Nordbotten, J.M, Celia, M. A.: Evaluation of the spread of acid gas plumes injected in deep saline aquifers in western Canada as an analogue to CO_2 injection in continental sedimentary basins. In: Rubin, E.S., Keith, D.W., Gilboy, C.F. (eds) Peer Reviewed Papers and Overviews, Proceedings of 7th International Conference on Greenhouse Gas Control Technologies, 5-9 September 2004, Vancouver, Canada. vol. 1, pp479–487. Elsevier (2005)

Bachu, S., Carroll, J.J.: In-situ phase and thermodynamic properties of resident brine and acid gases (CO_2 & H_2S) injected in geological formations in western Canada. In: Rubin E.S., Keith D.W., Gilboy C.F. (eds) Peer Reviewed Papers and Overviews, Proceedings of 7th International Conference on Greenhouse Gas Control Technologies, 5-9 September 2004, Vancouver, Canada, Vol. 1, pp449-457. Elsevier (2005)

Beck, J.L.: Convection in a box of porous material saturated with fluid. Phys. Fluids **15**(8), 1377–1383 (1972)

Caltagirone, J.-P.: Stability of a saturated porous media layer subject to a sudden rise in surface temperature: comparison between the linear and energy methods. Quart. J. Mech. Appl. Math. **33**, 47–58 (1980)

Carslaw, H.S., Jaeger, J.C.: Conduction of Heat in Solids, p. 185. Oxford University Press (1959)

Ennis-King, J.P., Paterson, L.: Role of convective mixing in the long term storage of carbon dioxide in deep saline formations, SPE paper 84340, ATCE 5–8 October 2003. Denver (2003)

Ennis-King, J.P., Preston, I., Paterson, L.: Onset of convection in anisotropic porous media subject to a rapid change in boundary conditions. Phys. Fluids **17**, 084107 (2005)

Foster, T.: Stability of a homogenous fluid cooled from above. Phys. Fluids **8**(7), 1249–1257 (1965a)

Foster, T.: Onset of convection in a layer of fluid cooled from above. Phys. Fluids **8**(10), 1770–1774 (1965b)

Foster, T.: Effect of boundary conditions on the onset of convection. Phys. Fluids **11**, 1257–1262 (1968)

Gerald C.F., Wheatley, P.O.: Applied Numerical Analysis, 4th edn. Reading, MA: Addison-Wesley (1989)

Hassanzadeh, H., Pooladi-Darvish, M., Keith, D.W.: Modeling of convective mixing in CO_2 storage. J. Can. Petroleum Technol. **44**(10), (2005)

Hassanzadeh, H.: Mathematical modeling of convective mixing in porous media for geological CO_2 storage. Dissertation, University of Calgary (2006)

Horton, C.W., Rogers, Jr., F. T., : Convection currents in porous media. J. Appl. Phys. **20**, 367–369 (1945)

Intergovernmental Panel on Climate Change (IPCC): Special report on Carbon Dioxide Capture and Storage. Cambridge University Press (2005)

Jhavery, B.S., Homsy, G.M.: The onset of convection in fluid layer heated rapidly in a time-dependent manner. J. Fluid Mech. **114**, 251–260 (1982)

Kaviany, M.: Onset of thermal convection in a saturated porous medium: experiment and analysis. Intern. J. Heat Mass Transfer **27**(11), 2101–2110 (1984)

Katto, Y., Masuoka, T.: Criterion for the onset of convective flow in a fluid in a porous medium. Intern. J. Heat Mass Transfer **10**, 297–309 (1967)

Kim, M.C., Kim, L.H., Choi, C.K.: The onset of convective motion in a horizontal fluid layer heated from below and cooled from above with constant heat flux. Int. Comm. Heat Mass Transfer **31**, 837–846 (2004)

Kim, M.C., Kim, S.: Onset of convective stability in a fluid-saturated porous layer subjected to time-dependent heating. Int. J. Heat Mass Transfer **32**(3–4), 416–424 (2005)
Kvernvold, D., Tyvand, P.: Dispersion effects on thermal convection in porous media. J. Fluid Mech. **99**(part 4), 673–686 (1980)
Lapwood, E.R.: Convection of a fluid in a porous medium. Proc. Cambridge Phil. Soc. **44**, 508–521 (1948)
Lick, W.: The stability of a fluid layer with time-dependent heating. J. Fluid Mech. **21**(part 3), 565–576 (1965)
Lindeberg, E.G.B, Wessel-Berg, D.: Vertical convection in an aquifer column under a gas cap of CO_2. Energy Convers. Manage. **38**, 229–234 (1996)
Mahler, E.G., Schechter, R.S, Wissler, E.H.: Stability of a fluid layer with time-dependent density gradients. Phys. Fluids **11**(9), 1901–1912 (1968)
Morrison, H.L., Rogers, Jr., F.T., Horton, C.W.: Convection currents in porous media, II. Observation of conditions at onset of convection. J. Appl. Phys. **20**, 1027–1029 (1949)
Morton, B.R.: On the equilibrium of a stratified layer of fluid. J. Mech. Appl. Math. **10**, 433–447 (1957)
Nield, D.A., Bejan, A.: Convection in Porous Media. Springer-Verlag, Second Edition, New York (1999)
Ozisik, M.N.: Heat Conduction, 2nd edn, p. 48. John Wiley & Sons (1993)
Riaz, A. Hesse, M., Tchelepi, A., Orr, Jr., F.: Onset of convection in a gravitationally unstable, diffusive boundary layer in porous media. J. Fluid Mech. **548**, 87–111 (2006)
Rubin, H.: Heat dispersion effect on thermal convection in a Porous medium layer. J. Hydrol. **21**, 173–185 (1974)
Tan, K.K., Thorpe, R.B.: The onset of convection caused by buoyancy during transient heat conduction in deep fluids. Chem. Eng. Sci. **51**, 4127–4136 (1996)
Tyvand, P.: Heat dispersion effect on thermal convection in anisotropic porous media. J. Hydrol. **34**, 335–342 (1977)
Wankat, P.C., Homsy, G.M.: Lower bounds for the onset of instability in heated layers. Phys. Fluids **20**, 1200–1201 (1977)
Weber, J.: Dispersion effect on buoyancy-driven convection in stratified flows through porous media. J. Hydrol. **25**, 59–70 (1975)
Xu, X., Chen, S., Zhang, Z.: Convective stability analysis of the long-term storage of carbon dioxide in deep saline aquifers. Advances in Water Resources **29**, 397–497 (2006)